Power Losses in Steel Pipe Delivering Very Large Currents

Bruce C. W. McGee and Fred E. Vermeulen, Members IEEE

Abstract— **This paper presents a Finite Difference Time Domain solution for the electromagnetic fields in ferromagnetic conducting steel pipes of the type used to deliver large currents for in-situ heating of heavy oil reservoirs and for in-situ environmental decontamination. A method is described whereby a single measured hysteresis loop can be used to deduce the family of hysteresis loops that governs the variable magnetic behaviour throughout the pipe wall. Hysteresis and eddy current losses are calculated and it is shown that hysteresis effects greatly alter the eddy current distribution and can more than triple the total power losses in the steel pipe when compared to the power losses that would be present if hysteresis effects are ignored and magnetic permeability is assumed constant.**

Index Terms— **Time dependent magnetic fields, Finite Difference Time Domain methods, Hysteresis modelling, Hysteresis nonlinearities, Eddy currents, Losses.**

I. Introduction

In-situ electrical heating has been shown to more than double production rates from heavy oil reservoirs and to significantly accelerate vapor phase extraction processes for decontamination of hydrocarbon polluted sites [1], [2]. These processes involve the delivery of currents of several hundred amperes for periods of many months through steel pipes that comprise the vertical and horizontal wells and lead to electrodes from where the current is conducted into the formation [3], [4]. The ability to predict power losses in these pipes is required so that their current carrying capacity may be determined, to design pipe cooling systems when required, and to predict the efficiency with which electrical power is delivered to the formation and converted to heat. The steel piping is ferromagnetic and determination of total power losses must account for eddy current and hysteresis losses.

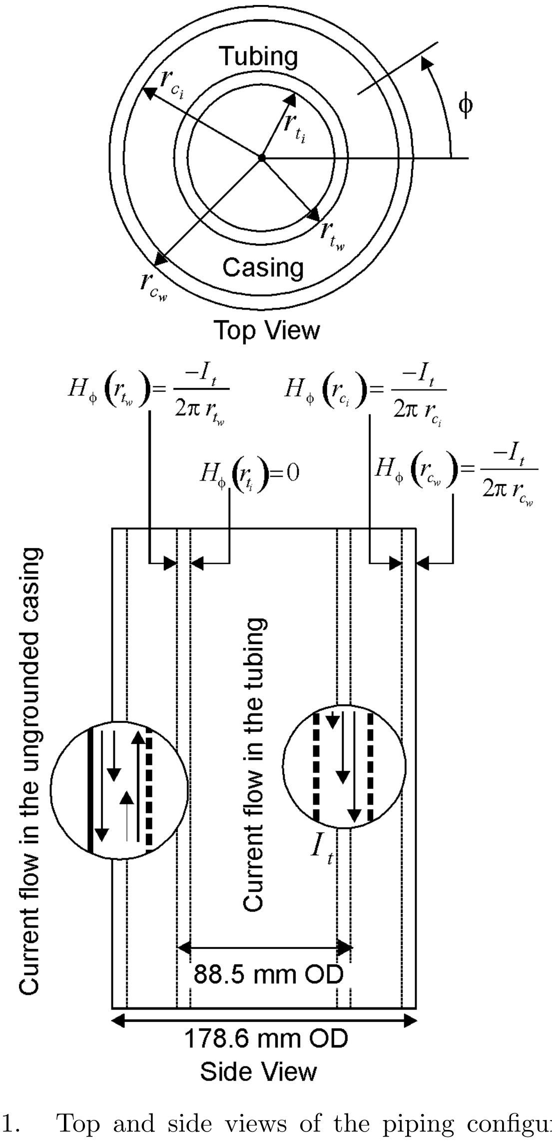

Fig. 1. Top and side views of the piping configuration for power delivery. The tubing current I_t flows downward in the negative z-direction. The magnetic field strengths H_ϕ are given at all interior and exterior steel surfaces, and the directions and amplitudes of current densities are indicated.

An analytic treatment of eddy current losses in steel piping of constant magnetic permeability has been given by Loga et. al. [5]. When magnetic hysteresis is present the analytic determination of

B. McGee is with McMillan-McGee Corp., Calgary, Alberta, CANADA. E-mail: mcgee@mcmillan-mcgee.com

F. Vermeulen is with the Department of Electrical and Computer Engineering, University of Alberta, Edmonton, Alberta, CANADA. E-mail: vermeulen@ee.ualberta.ca

losses is not possible due to the very non-linear relationship between the magnetic induction $\vec{\mathbf{B}}$ and the magnetic field strength $\vec{\mathbf{H}}$. In this paper the Finite Difference Time Domain (FDTD) numerical method is used to solve the applicable Maxwell's equations. This method is able to deal with the transitory response of the magnetization process and account for the fact that the steady state magnetization of the steel pipe is highly dependent on the history of magnetization starting from initial conditions.

The numerical approach in this paper partially parallels that of *Zakrzewski and Pietras* [6]. The significant difference, in addition to solving a cylindrical rather than a planar problem, is that our method of geometrically constructing a family of hysteresis loops uses only a *single* experimentally measured hysteresis loop and the peak magnetization curve, rather than requiring extrapolation between data points of *several* experimentally derived hysteresis loops. Also, the electric field strength in the interior of the material is calculated using the integral form of Maxwell's equations rather than the point form.

Figure 1 shows the piping configuration in the vertical part of a basic oil wellbore equipped for electrical heating. Oil flows to the surface in the region interior to the tubing, and the current is delivered in the steel of the tubing to the oil reservoir. For the problem analysed here the casing is ungrounded and electrically isolated from the tubing. Current flow in the tubing induces a circulating current in the casing. At the interior surface of the casing the induced current flows in a direction opposite to that of the current in the tubing. The induced return current flows in the opposite direction at the casing exterior.

In this paper the eddy current and hysteresis losses are analysed in the casing. The solution method that is presented is, however, equally valid for the analysis of losses in the tubing.

Figure 1 shows directions and amplitudes of current flow in tubing and casing and the magnetic field strengths H_ϕ, derived from Ampere's law, are given for all tubing and casing surfaces.

Figure 2 shows the magnetic and electric field strengths E_z and H_ϕ, and the Poynting vectors $\vec{S}$ for an element of casing. The interior and exterior surfaces of the casing are located at radii r_{ci} and r_{cw}, respectively. For simplicity, in the work that follows, r_{ci} and r_{cw} are replaced by r_i and r_w.

With reference to Figure 2, the following assumptions are made:

1. The pipe is long enough so that end effects can be neglected, and the frequency of the excitation is sufficiently low that wavelength effects are negligible. It follows that there is no variation of any field quantity along the axial direction z.
2. The tubing current has cylindrical symmetry, and, for the purpose of calculating the induced current in the casing, is replaced by a line current I_t on the axis of the casing ar $r = 0$. It follows that the field solution is independent of ϕ.

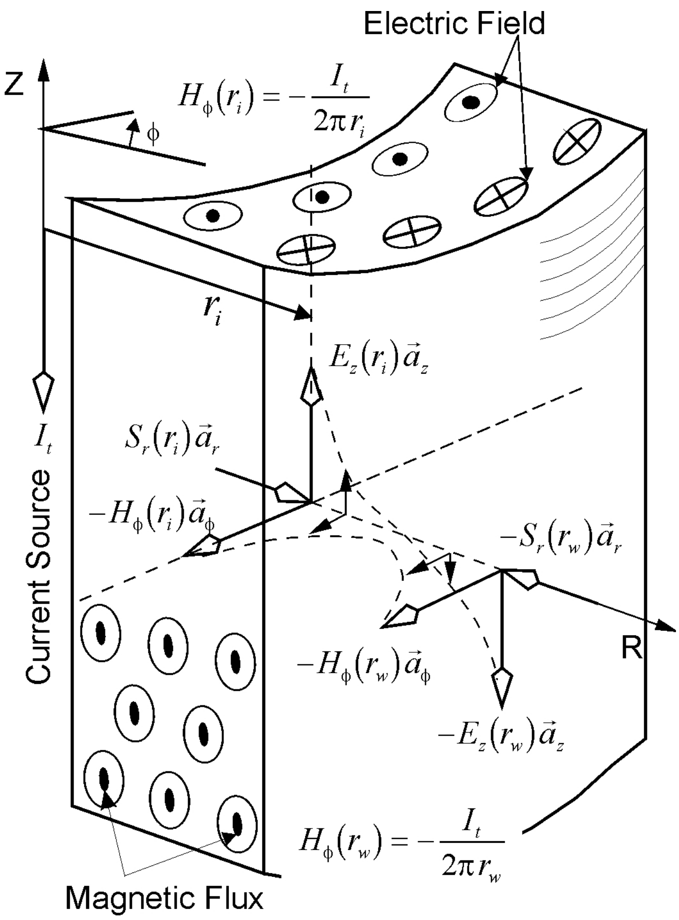

Fig. 2. The electromagnetic problem in the casing. Shown are the electric and magnetic field strengths, E_z and H_ϕ, and the Poynting vetor $\vec{S}$.

Within the steel the only components of electric and magnetic field strengths are E_z and H_ϕ, and both of these vary in amplitude and phase in the radial direction. The Poynting vectors $\vec{S}$ are directed into the casing at both interior and exterior surfaces.

Once solutions for E_z and H_ϕ have been obtained, their values at the interior and exterior casing surfaces can be used to calculate the total power losses in the casing using Poynting's theorem. The relative contributions to these losses by eddy currents and hysteresis losses must be obtained by integrating local values of these losses throughout the volume of the casing.

II. Finite Difference Time Domain Solution

A partial differential equation in terms of $H_\phi(r)$ is derived from Maxwell's equations. Finite differencing techniques are applied to the derivatives appearing in this equation, and the non-linear relationship between **B** and **H** is defined using hysteresis loops. Boundary conditions are invoked and the solution for the magnetic field strength is obtained. Then, using Ampere's law, the electric field strength is derived from the magnetic field strength.

A. Partial differential equation for the magnetic field strength

Maxwell's equations are

$$\nabla \times \vec{\mathbf{E}} = -\frac{\partial \vec{\mathbf{B}}(\vec{\mathbf{H}})}{\partial \mathbf{t}} \tag{1}$$

$$\nabla \times \vec{\mathbf{H}} = \varepsilon \frac{\partial \vec{\mathbf{E}}}{\partial \mathbf{t}} + \sigma \vec{\mathbf{E}} \tag{2}$$

The scalar equivalent of the partial derivative on the R.H.S. of Equation 1 can be written as

$$\frac{\partial B(H)}{\partial t} = \frac{d B(H)}{d H} \frac{\partial H}{\partial t} \tag{3}$$

Now define

$$\mu(H) \equiv \frac{d B(H)}{d H} \tag{4}$$

and directly substitute Equations 3 and 4 into Equation 1.

At 60 *Hz* the magnitude of the conduction current is much greater than the magnitude of the displacement current, and Equations 1 and 2 are rewritten as

$$\nabla \times \vec{\mathbf{E}} = -\mu(\vec{\mathbf{H}}) \frac{\partial \vec{\mathbf{H}}}{\partial \mathbf{t}} \tag{5}$$

$$\nabla \times \vec{\mathbf{H}} = \sigma \vec{\mathbf{E}} \tag{6}$$

Equation 6 is expanded as

$$\left(\frac{1}{r}\frac{\partial H_z}{\partial \phi} - \frac{\partial H_\phi}{\partial z}\right)\vec{a}_r + \left(\frac{\partial H_r}{\partial z} - \frac{\partial H_z}{\partial r}\right)\vec{a}_\phi + \frac{1}{r}\left(\frac{\partial (rH_\phi)}{\partial r} - \frac{\partial H_r}{\partial \phi}\right)\vec{a}_z = \sigma \vec{\mathbf{E}} \tag{7}$$

Since the only field components present are H_ϕ and E_z, and these are independent of ϕ, Equation 7 becomes

$$\frac{1}{r}\frac{\partial (r H_\phi)}{\partial r} = \sigma E_z \tag{8}$$

Similarly, Equation 5 reduces to

$$\frac{\partial E_z}{\partial r} = \mu(H_\phi)\frac{\partial H_\phi}{\partial t} \tag{9}$$

From Equations 8 and 9 it follows that,

$$\frac{\partial^2 H_\phi}{\partial r^2} + \frac{1}{r}\frac{\partial H_\phi}{\partial r} - \frac{H_\phi}{r^2} = \sigma\mu(H_\phi)\frac{\partial H_\phi}{\partial t} \tag{10}$$

Equation 10 is a diffusion type equation and describes the distribution of the magnetic field strength in the steel pipe. Equation 10 is discretized and numerically solved. Specification of the magnetic field strengths at the boundaries determines whether the solution is for the tubing or ungrounded casing. Appropriate boundary conditions are shown in Figure 1.

Once the magnetic field strength H_ϕ has been determined, Ampere's law

$$\oint_C \vec{\mathbf{H}} \cdot \mathbf{d}\vec{\mathbf{l}} = \int_{\mathbf{S}} \sigma \vec{\mathbf{E}} \cdot \mathbf{d}\vec{\mathbf{S}} \tag{11}$$

is used to determine the electric field strength in the steel pipe.

B. Numerical Solution for H_ϕ and E_z

The independent variables of Equation 10 are discretized and a solution for H_ϕ is found at a finite number of node points in space and at specific intervals in time. Figure 3 shows the solution

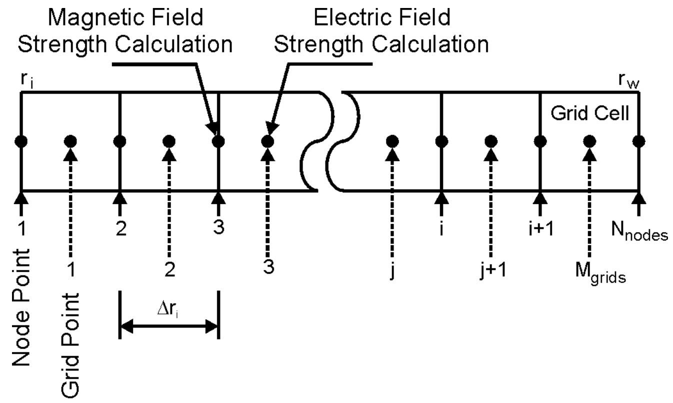

Fig. 3. Grid system, consisting of node and grid points, adopted for the finite difference time domain numerical calculations.

space, which consists of the casing volume between r_i and r_w. The node points, at which H_ϕ is calculated, are on the boundaries of the grid cells. The grid points, at which E_z is calculated by use of Ampere's law, lie at the center of the grid cells.

The fully implicit *Crank-Nicholson* solution method was chosen for which discretization of Equation 10 leads to

$$a_i H_{i-1}^{n+1} + (b_i + 2d_i^n)\, H_i^{n+1} + c_i H_{i+1}^{n+1} = \\ - a_i H_{i-1}^{n} + (2d_i^n - b_i)\, H_i^{n} - c_i H_{i+1}^{n} \quad (12)$$

where the subscript ϕ has been deleted, superscripts denote time levels, and where the truncation error is $O(\Delta t^2 + \Delta r^2)$. Here

$$\begin{aligned} a_i &= \frac{1}{\Delta r^2} - \frac{1}{2r_i\Delta r} \\ b_i &= -\frac{1}{r_i^2} - \frac{2}{\Delta r^2} \\ c_i &= \frac{1}{\Delta r^2} + \frac{1}{2r_i\Delta r} \\ d_i^n &= -\frac{\sigma_i \mu_i^n}{\Delta t} \end{aligned} \quad (13)$$

In this solution method the magnetic field strength at every node point is obtained *implicitly* from the magnetic field strength at the previous time level. The method is unconditionally stable for all values of Δt and Δr. The explicit solution method, in which the magnetic field strength is obtained *explicitly* from the values at the previous time level, was also considered but deemed unsuitable. The explicit scheme suffers from the restriction that $\frac{a_i}{d_i^n} < \frac{1}{2}$ for stability. For typical properties of steel and a reasonable Δr of 0.1 mm this will require a time step of less than 0.1 $\mu\, sec$ to ensure stability, which renders the technique impractical.

The steady state solution for H depends on the history of magnetization of the material, which must be accounted for as Equation 12 is stepped through time, starting from initial conditions when H is set to zero and the initial value of magnetic permeability, μ_i^1, is set to the initial value of magnetic permeability for the material at every node point. The matrix of coefficients representing the tridiagonal system of equations arising from Equation 12 is therefore continually recomputed as time advances, using the current value of H at every node point of the problem domain to update every local value μ_i^n. Each node point experiences a different magnetization history, and, once steady state is reached, is associated with a different steady state hysteresis loop.

Discretization of Ampere's law, Equation 11, leads to the equation for the z-directed electric field strength

$$E_{i+1/2}^{n+1} = \frac{2\left(H_{i+1}^{n+1}R_{i+1} - H_i^{n+1}R_i\right)}{\sigma \cdot \left(R_{i+1}^2 - R_i^2\right)} \qquad 1 \le i \le N-1 \quad (14)$$

The electric field strengths at the inner and outer boundary node points are, respectively, obtained by linear extrapolation from the electric field strengths at the nearest grid points.

C. The magnetization process for the steel pipe

It is assumed that the steel pipe is initially demagnetized and that the initial conditions that exist in every grid cell correspond to the origin of Figure 4. As the magnetic field strength increases in time, magnetization initially follows the *peak magnetization curve.* When the magnetic field strength has reached a maximum at the downer turn around point, defined numerically by $H_i^{n+1} < H_i^n$, demagnetization follows along the curve called the *downer loop.*

The magnetic field strength reaches a minimum at the *upper turn around point*, defined numerically by $H_i^{n+1} > H_i^n$. Remagnetization now occurs along the *upper loop* until the *downer turn around point* is reached again, completing a single cycle

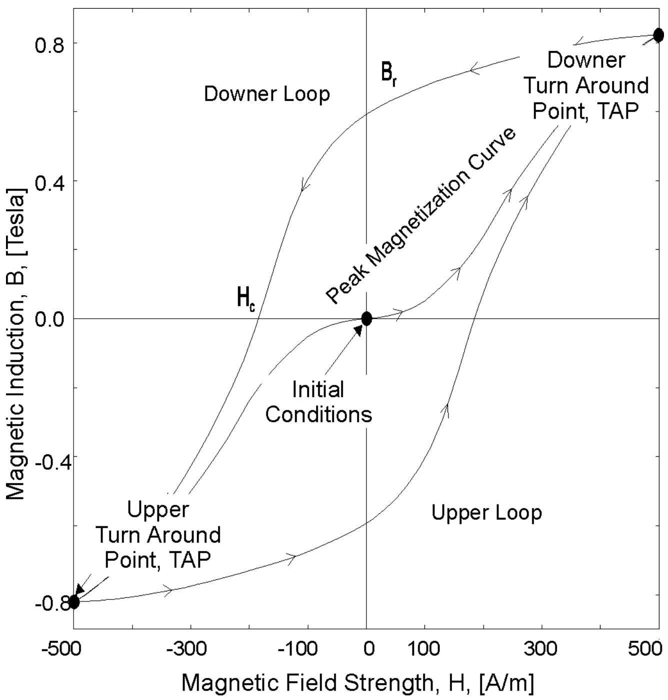

Fig. 4. Characteristics of the magnetization process within a single grid cell of width Δr_i.

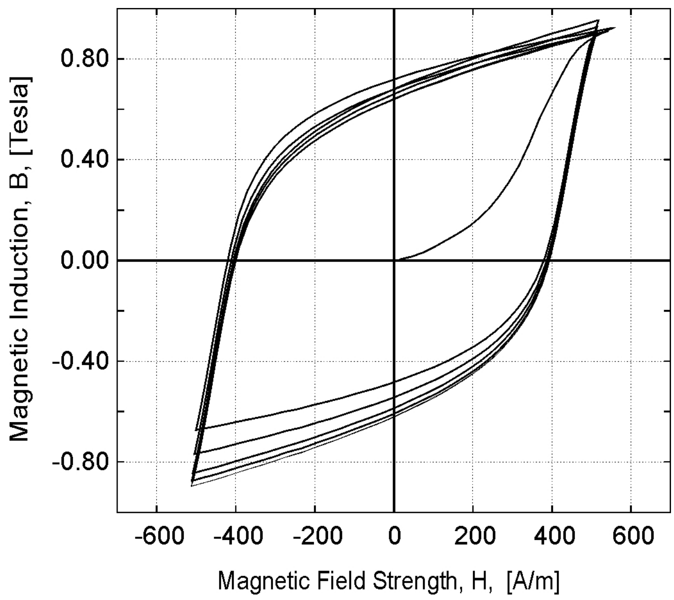

Fig. 5. The magnetization of a grid cell during the transient period.

of magnetization. The magnetization process continues along *downer* and *upper* loops during each cycle of the applied magnetic field strength.

Magnetization along the peak magnetization curve only occurs once from the initial condition of zero magnetization. During the transient period, the two turn around points change location from one cycle to the next, and, except for the initial downer turn around point, do not lie on the peak magnetization curve. As steady state is reached the two turn around points locate on the peak magnetization curve, and the downer and upper loops become symmetrical.

The downer and upper loops shown in Figure 4 correspond to steady state. In Figure 5 the upper and downer loops are traced for ten cycles during the transient period, and it is seen that steady state is approached after approximately five cycles.

D. Distance factor method for constructing the hysteresis loops

To determine the magnetization for each grid cell by solution of Equation 10 requires a general method for generating hysteresis loops. The method presented here is an extension of a method developed by *Talukdar and Bailey* [7], who developed a scaling procedure using a *distance factor*.

The *distance factor* approach requires a maximum hysteresis loop for the magnetic material which is usually obtained experimentally. For the *Talukdar and Bailey* approach the maximum hysteresis loop *must* extend to the magnetic saturation of the material. This condition is not necessary for the *distance factor* method presented in this paper. Our only requirement is that the extremum of the maximum hysteresis loop be greater than the maximum value of the applied magnetic field strength for the problem being solved.

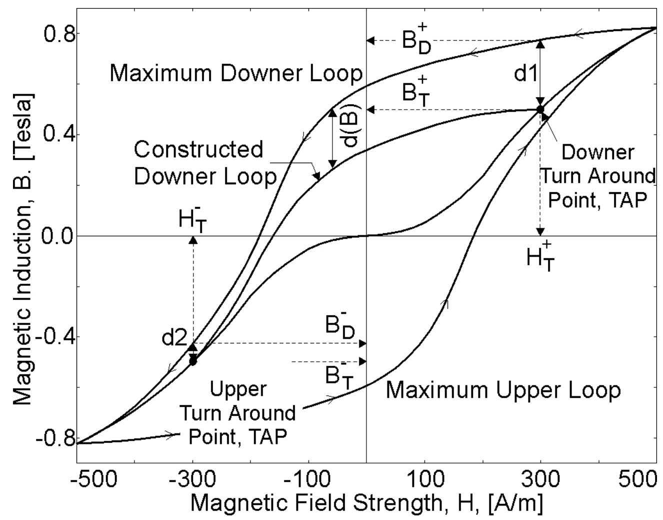

Fig. 6. Method for constructing hysteresis loops used in this paper. The very first turn around point lies on the peak magnetization curve but subsequent turn around points generally do not until steady state is reached.

With reference to Figure 6, our approach for constructing a hysteresis loop for an arbitrary value of maximum applied magnetic field strength is as follows:

1. The *downer turn around point* is defined by the coordinate, (H_T^+, B_T^+) and is located on the *peak magnetization curve*. When the magnetic field strength reaches the *downer turn around point*, determine the vertical distance from the *maximum downer loop* to the *downer turn around point*, $d_1 = B_D^+ - B_T^+$.

2. Define a *hypothetical upper turn around point* as the mirror image $(H_T^-, B_T^-) = (-H_T^+, -B_T^+)$, and which is also located on the peak magnetization curve. The vertical distance from the peak magnetization curve to this second point is $d_2 = B_D^- - B_T^-$. Now define a distance factor

$$d(B) = d_2 + \frac{d_1 - d_2}{B_T^+ - B_T^-} \left(B - B_T^-\right) \qquad (15)$$

3. The *constructed downer loop* is now calculated for decreasing magnetic field strength from

$$B_{cd}(H) = B_d(H) - d(B)$$

where $B_{cd}(H)$ is the magnetic induction for the constructed downer loop and $B_d(H)$ is the magnetic induction corresponding to the maximum downer loop.

4. When the *actual* upper turn around point is reached, which, during the first few cycles of excitation is *not* located on the peak magnetization curve at (H_T^-, B_T^-), define a *hypothetical downer turn around point* as the mirror image in the first quadrant of the *actual* upper turn around point. The constructed upper loop is now calculated for increasing magnetic field strength using a new distance factor $d(B)$ defined by an equation analogous to Equation 15.

It is noted that the method of *Talukdar and Bailey* forces the constructed downer loop and constructed upper loop to be symmetrical from the onset, a condition normally associated with steady state conditions. The method presented here is not subject to this constraint and hence the magnetization process through the transient period can be modelled

An advantage of using the *distance factor* method presented here, is that it is not necessary to obtain a maximum hysteresis loop that extends to the magnetic saturation of the material. This is an important experimental consideration since magnetic saturation for oil-field steel tubulars typically occurs at very large magnetic field strengths and practical values for the applied magnetic field strength are much less than at saturation conditions. Since it is desirable to use a maximum hysteresis loop that is close to the applied magnetic field strength to improve on the accuracy of the electromagnetic field calculations, the *distance factor* method presented in this paper was developed.

Figure 7 depicts the the process of magnetization within the steel casing at steady state conditions calculated using our *distance factor* method. The magnetic field strengths and areas bounded by the hysteresis loops decrease with increasing depth. The steady state magnetization process in each grid block is described by a unique hysteresis loop.

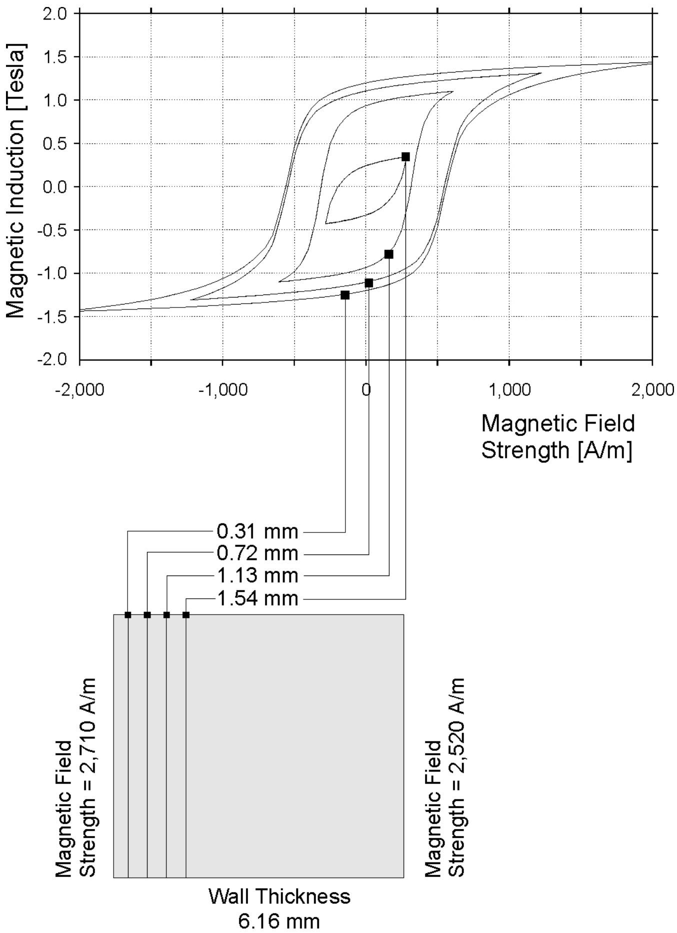

Fig. 7. Hysteresis loops at various distances from the interior surface of the casing calculated using our numerical model. The tubing current is 1,000 A RMS.

III. Power Losses in the Steel Pipe

A. Loss Calculations

The impact of hysteresis on the total power losses in the steel pipe is determined and the relative contributions of hysteresis losses and eddy current losses are obtained. An experimentally measured hysteresis loop for a sample of typical oil field production casing is used to generate the family of hysteresis loops required for the calculation of the electromagnetic fields, using the distance factor method. The analysis is for the ungrounded casing in the vertical section of the wellbore. The same analysis can be used to determine the losses in the tubing by applying the appropriate boundary conditions for the magnetic field strength at the inner and outer tubing surfaces, as stated in Figure 1.

The total time average power dissipated in unit length of casing is obtained by summing the Poynting vector time average power flow into the casing through its inner and outer surfaces, and is

$$P = -\frac{2\pi r_i}{T}\int_0^T E_z(r_i,t)\,H_\phi(r_i,t)\,dt + \frac{2\pi r_w}{T}\int_0^T E_z(r_w,t)\,H_\phi(r_w,t)\,dt \quad (16)$$

Hysteresis losses per unit length are

$$P_h = \frac{2\pi}{T}\int_{r_i}^{r_w}\oint_{B_\phi(0)}^{B_\phi(T)} H_\phi(r,B_\phi)\,dB_\phi\,r\,dr \quad (17)$$

and the eddy current losses per unit length are

$$P_{ec} = \frac{2\pi}{T}\int_{r_i}^{r_w}\int_0^T \sigma\,E_z^2(r,t)\,r\,dr\,dt \quad (18)$$

P_h and P_c must sum to the total power dissipated, P.

B. Magnetic properties of the casing and tubing

Casing and tubing of pipe type K-55, which is commonly used in oil field operations, was obtained from *Texaco Canada Petroleum Inc.* The casing, for which power loss calculations are presented, has radii $r_i = 83.2mm$ and $r_w = 89.3mm$, and is commonly referred to as 7" casing.

A sample of these materials was sent to *LDJ Electronics, Inc.* in Troy, Michigan, USA, for hysteresigraph testing to obtain several maximum hysteresis loops for use in constructing general hysteresis loops using the *distance factor* method. Figure 8 shows several measured hysteresis loops. Small adjustments to the experimental data are required to ensure that the *upper maximum loop* and *downer maximum loop* are symmetrical about the origin, that the ends of these loops coincide with the *peak magnetization curve*, and that the *peak magnetization curve* passes through the origin and is also symmetrical.

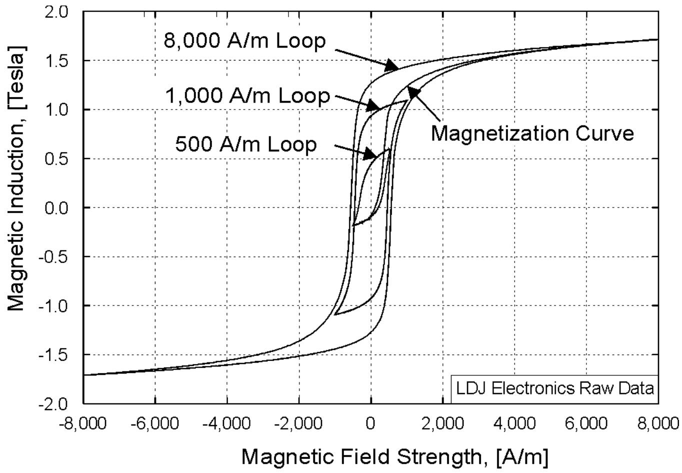

Fig. 8. Hysteresis data for the 7" casing obtained using a hysteresigraph test from *LDJ Electronics Inc.*

The experimental data was also filtered to ensure that the magnetic induction is monotonically increasing for the *upper loop* and monotonically decreasing for the *downer loop*. Without filtering negative or zero values for μ_r may be encountered during numerical calculations as shown in Figure 9. Figure 9 shows the relative permeability μ_r derived by numerical evaluation of the slopes of the experimental 1,000 A/m hysteresis loop. This data was arbitrarily curve fit using a cubic spline method to generate the filtered data, also shown in Figure 9. Several hysteresis loops for the 7" casing, constructed by the distance factor method, are shown in Figure 10. The pipe properties and runtime data for the power loss calculations are shown in Table I. In this table the initial relative permeability μ_{ro} is the relative magnetic permeability measured on the magnetization curve for small magnetic field strengths H.

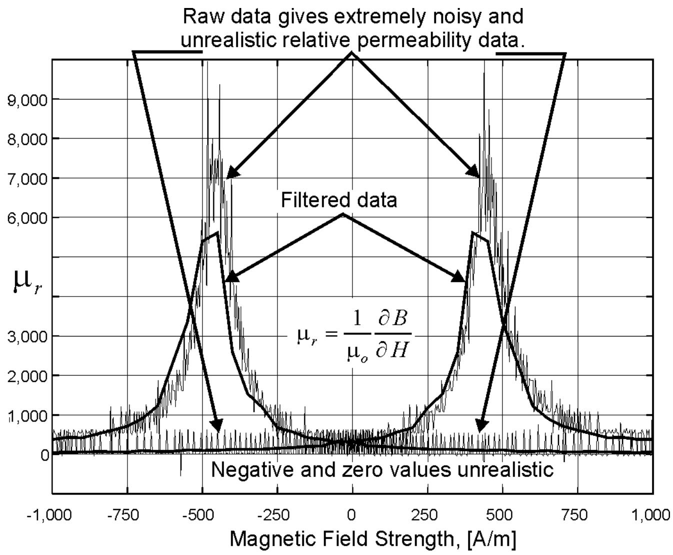

Fig. 9. Comparison of the relative permeability μ_r calculated using raw data with filtered values of μ_r for one complete traversal of the measured 1,000 A/m hysteresis loop.

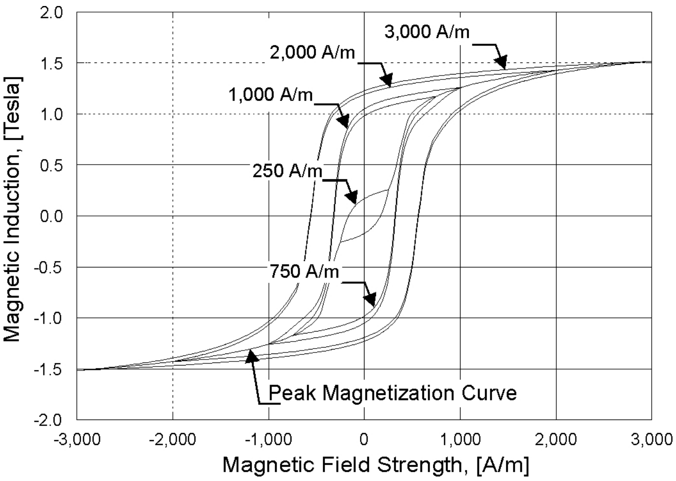

Fig. 10. Several constructed hysteresis loops for the casing based on the *LDJ Electronics Inc.* tests and calculated using the *distance factor* method. The 1,000 A/m hysteresis loop is experimentally measured.

C. *Impact of hysteresis on the distribution of the EM-Fields and power losses in steel pipe*

The effects of hysteresis on the distribution of eddy currents and losses in the casing in the vertical section of the wellbore are analysed for a tubing current of 500 *A RMS*, which produces magnetic field amplitudes of 1,353 A/m and 1,260 A/m at the interior and exterior surfaces, respectively.

Figures 11 and 12 compare the *RMS* values of electric and magnetic field strengths in the 7" casing with and without hysteresis effects. For the latter relative permeability is assumed constant

Data	Symbol	Value
Casing Properties		
Inner radius	r_i	83.2 mm
Outer radius	r_w	89.3 mm
Initial relative permeability	μ_{ro}	269.0
Electrical conductivity	σ_s	7.3 $\times 10^6$ S/m
Run Time Data		
Peak current	I_p	Varies, A
Peak magnetic field	$H(r_i)$	Varies, A/m
Frequency	f	60.0 Hz
Size of time step	Δt	34.7 μsec
Size of grid block	Δr	0.2 mm
Number of grid nodes	N_{nodes}	31 - 61
Time steps per cycle	N	480

TABLE I
CASING PROPERTIES AND RUNTIME DATA FOR POWER LOSS CALCULATIONS.

at $\mu_{ro} = 269.0$. The fields are severely distorted when hysteresis is present. A different hysteresis loop prevails at every radial location in the casing.

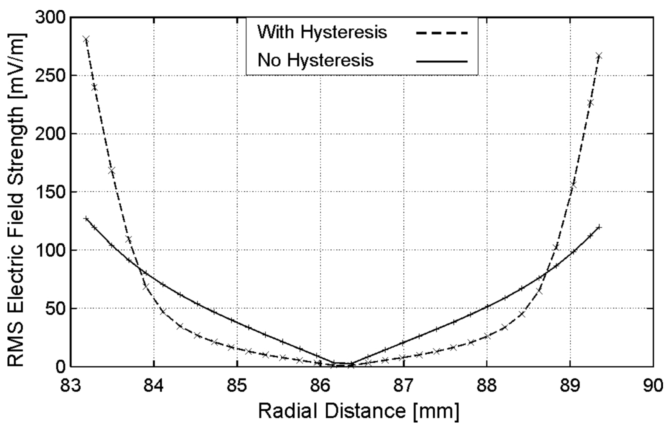

Fig. 11. The effect of hysteresis on the distribution of the electric field strength for the 7" steel casing for the case when the current in the centralized tubing is 500 A RMS at 60 Hz.

The redistribution of the electric field strength towards the interior and exterior surfaces when hysteresis is present results in an eddy current loss that is more than twice as large as when no hysteresis is present. In addition, the magnitude of the hysteresis loss is comparable to the eddy current loss in the pipe when hysteresis is not con-

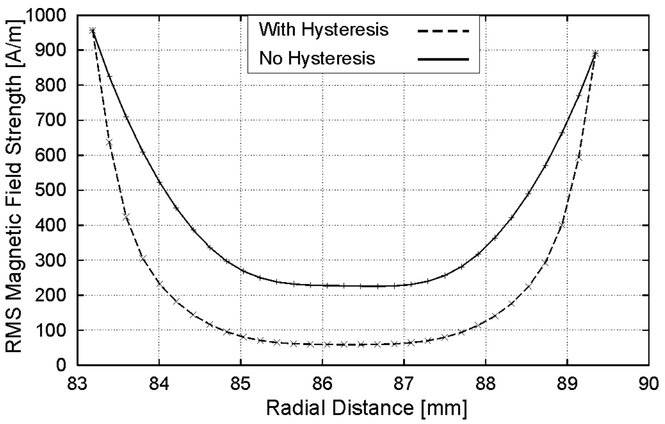

Fig. 12. The effect of hysteresis on the distribution of the magnetic field strength for the 7" casing for the case when the current in the centralized tubing is 500 A RMS at 60 Hz.

sidered. Thus, for this typical example, where the current in the centralized tubing is 500 *A RMS* *the overall impact of hysteresis is to increase the total power losses approximately three fold.*

As shown in Figure 11, hysteresis forces the current to flow very near the surfaces. The skin depth δ for the cylindrical 7" casing, with no hysteresis, is estimated from Figures 11 and 12 as 1.53 mm. The skin depth when hysteresis is present is approximately 0.54 mm.

The power losses are summarized in Table II. The data shows that the presence of hysteresis causes a very large increase in power losses and that its effects cannot be overlooked in the design of the power delivery system for electrical heating in oil field or environmental applications.

Data	Symbol	Value
Losses without Hysteresis		
Poynting Power	$P(r_i)$	46.6 W/m
	$P(r_w)$	44.2 W/m
Total Power Losses	P	90.8 W/m
Eddy Current Loss	P_{ec}	89.3 W/m
Hysteresis Loss	P_h	0.0 W/m
% Hysteresis Loss		0.0
RMS Electric Field	$E_z(r_i)$	127.5 mV/m
Strengths at surfaces	$E_z(r_w)$	119.9 mV/m
Skin Depth	δ	1.53 mm
Losses with Hysteresis		
Poynting Power	$P(r_i)$	121.2 W/m
	$P(r_w)$	115.4 W/m
Total Power Losses	P_t	236.6 W/m
Eddy Current Loss	P_{ec}	155.4 W/m
Hysteresis Loss	P_h	77.0 W/m
% Hysteresis Loss		33.1
RMS Electric Field	$E_z(r_i)$	257.7 mV/m
Strengths at surfaces	$E_z(r_w)$	245.5 mV/m
Skin Depth	δ	0.54 mm

TABLE II
LOSSES IN THE 7" CASING WHEN THE CURRENT IN THE TUBING IS 500 A RMS AT 60 HZ.

D. *Hysteresis and eddy current losses as a function of the current conducted in the centralized tubing*

The current in the tubing was varied between 40 and 1,000 *A RMS* to evaluate hysteresis, eddy current, and total power losses as a function of increasing magnetic field strength in the casing. Figure 13 shows the losses as a function of current magnitude in the tubing. It is evident that the relative importance of hysteresis does not always increase with an increase in the current carried in the tubing. Indeed, in this example the largest relative contribution of the hysteresis losses to the total power losses occurs at a much lower magnetic field strength than the saturation magnetic field strength. The diminishing relative contribution from hysteresis losses at higher tubing currents is due to the fact that the area enclosed by each hysteresis loop increases rather slowly as the peak magnetic field strength increases beyond a certain value. As a result the increase in eddy current losses, which depends on the square of the current, dominates at higher currents.

In addition to numerically computed losses Figure 13 also shows losses obtained experimentally. A four meter long section of the 7" type K-55 casing described in Table I was mounted in the laboratory. A five meter long type K-55 section of tubing of inside and outside radii of 38.1 and 44.3 mm, respectively, was centered within the casing. The entire apparatus was thermally insulated and the temperatures of casing and tubing were monitored with thermocouples. Uniform circumferential cable contact was made at both ends of the tubing so that current would uniformly enter and exit. Tubing current was supplied from a variable voltage transformer connected to a water-cooled high current transformer. Power dissipated in the ungrounded casing by induced circulating currents was calculated from the measured initial time rate of change of casing temperature, and the known casing heat capacity, $3.7 \cdot 10^6\ J/m^3\ °C$, at tubing currents ranging from 150 to 900 $A\ RMS$. As seen from Figure 13, the numerically computed values and measured values are in close agreement. A full description of the experiment is given elsewhere [3].

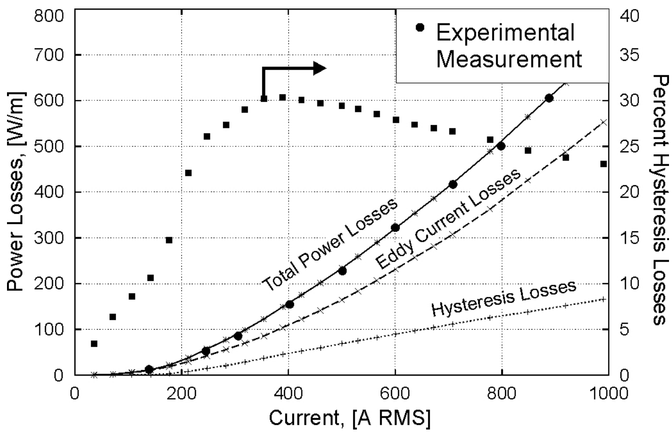

Fig. 13. Computed and measured power losses in the 7" casing as a function of current in the tubing.

IV. Conclusions

A FDTD solution of Maxwell's equations was developed to study the impact of hysteresis upon the delivery losses in a current carrying steel pipe. A method is described whereby a single measured hysteresis loop is used to deduce the family of hysteresis loops that characterizes the variable magnetic behaviour throughout the material. Hysteresis and eddy current losses in the steel pipe commonly used for power delivery for in-situ heating in oil fields and for environmental remediation are significant, and limit the magnitude of the current that can be used in the electrical heating process. To permit using larger currents special non-magnetic material, such as aluminum, may be required in the tubing and casing to eliminate the effect of hysteresis.

The analysis of the hysteresis and eddy current losses in the commonly used 7" casing indicates that *hysteresis losses can account for up to 25 % of the total losses* at relatively small current levels of 250 *A RMS*. At current levels between 250 and 400 *A RMS* hysteresis losses can account for as much as 30 % of the total losses. Also, hysteresis effects will cause a re-distribution of current in the casing which increases eddy current losses and can result in total delivery losses that are *three* times greater than if hysteresis were not present and with relative magnetic permeability assumed constant at its initial value μ_{ro}. Numerically computed values of total power delivery losses are in close agreement with measured values.

Acknowledgments

The authors would like to acknowledge the Natural Sciences and Engineering Research Council of Canada for supporting this work and Texaco Canada Inc. for donating the casing and tubing samples.

References

[1] H. Michael Buettner and William D. Daily, "Cleaning Contaminated Soil Using Electrical Heating and Air Stripping," *Journal of Environmental Engineering*, pp. 580–589, August, 1995.

[2] J. O. S. Pizarro and O. V. Trevisan, "Electrical Heating of Oil Reservoir - Numerical Simulation and Field Test Results," *Journal of Petroleum Technology*, pp. 1320–1326, October, 1990.

[3] Bruce C. W. McGee, *Electrical Heating of Heavy Oil Reservoirs Using Horizontal Wells*, Ph.D. thesis, University of Alberta, Edmonton, Alberta, Canada, 1998.

[4] C. P. Stroemich, F. E. Vermeulen, F. S. Chute, and E. Sumbar, "Wellbore Power Transmission For In-Situ Electrical Heating," *Alberta Oil Sands Technology and Research Journal of Research*, vol. 6, pp. 273–294, 1990.

[5] T. Loga, F. S. Chute, and F. E. Vermeulen, "Simple Finite Element Solutions for Eddy Current Losses in Pipe-Type Cables," *Applied Computational Electromagnetic Society*, vol. 10, no. 2, pp. 102–109, July 1995.

[6] K. Zakrzewski and F. Pietras, "Method of Calculating the Electromagnetic Field and Power Losses in Ferromagnetic Materials, Taking Into Account Magnetic Hysteresis," *Proc. IEE*, vol. 118, no. 11, November, 1971.

[7] Sarosh N. Talukdar and James R. Bailey, "Hysteresis Models for System Studies," *IEEE Transactions on Power Apparatus and Systems*, vol. PAS-95, no. 4, pp. 1429–1434, July-August, 1976.

Bruce C. W. McGee is president of McMillan-McGee Corporation, which is currently involved with several field electrical heating projects. He received his B.Sc. in 1980, M.Eng. in 1984, and Ph.D. in 1998 from the University of Alberta, all in electrical engineering, and M.E. Chem. E. in 1989 from the University of Calgary. He has extensive experience in the oil and gas and environmental industries. Born April 22, 1957

Fred E. Vermeulen is Professor of Electrical and Computer Engineering at the University of Alberta. He received his B.Sc. from the University of Alberta, his M.A.Sc. from the University of British Columbia, and a Ph.D. degree from the University of Alberta, all in electrical engineering. He was a Natural Sciences and Engineering Research Council Postdoctoral Fellow at the European Organization for Nuclear Research in Geneva from 1966 to 1967. His teaching and research are in the area of applied electromagnetics. He has a particular interest in in-situ electromagnetic heating for enhanced oil recovery and environmental remediation. He is a recipient of the IEEE Centennial Medal and was made a 3M Teaching Fellow in 1990, and received the 1999 Medal for Distinction in Engineering Education from the Canadian Council of Professional Engineers. Born May 13, 1938.